

Fluorescent Gels



A Biomimetic Supramolecular Approach for Charge Transfer between Donor and Acceptor Chromophores with Aggregation-Induced Emission

Jing-Yu Chen,^[a] Gajanan Kadam,^[b] Akhil Gupta,^{*,[a]} Anuradha,^[c] Sheshanath V. Bhosale,^{*,[d]} Fei Zheng,^[e] Chun-Hua Zhou,^[e] Bao-Hua Jia,^[e] Dipak S. Dalal,^[b] and Jing-Liang Li^{*,[a]}

Abstract: Supramolecular assembly of chromophores with inherent resistance to aggregation-induced self-quenching is significant to applications such as chemical sensing and organic light emitting diodes (OLEDs). In this work, molecular gels with aggregation-induced emission (AIE) are constructed by simply coassembling AIE chromophores (electron donor or acceptor) with a nonfluorescent molecular gelator. The binary gels are fluorescent even at very low concentrations of the AIE chromophores, indicating that the rotation

of their aromatic cores is restricted in the gel network. In tertiary gels, the fluorescence of the donor chromophore can be efficiently reduced by the acceptor chromophore through a combination of static and dynamic quenching process, via charge transfer from the donor to the acceptor. This work demonstrates a convenient approach to fabricate a supramolecular charge transfer system using an AIE donor and acceptor.

Introduction

Charge transfer is essential for many processes both in nature (e.g., photosynthesis) and in artificial systems such as solar cells and organic light emitting diodes (OLEDs).^[1] The efficiency of the processes depends on precise molecular organization of the donor and acceptor. For example, in natural light harvesting systems, high energy conversion efficiencies are achieved through formation of elegant supramolecular light harvesting complexes in which donor and acceptor molecules are properly organized on protein scaffolds for charge transfer and transport.^[2] The high efficiency of the natural charge transfer systems inspired the design of biomimetic supramolecular struc-

tures such as nanofibers/nanorods, to improve the efficiency of artificial systems.^[3] In organic solar cells (OSCs), nanowire/fiber structures provide a path for charge transport. For example, it has been reported that the presence of nanowires provides an efficient hole transporting network with a hole mobility 70–100 times higher than those without nanowire structures.^[4] Consequently, a power conversion efficiency higher than 10% was achieved.^[4a] Nevertheless, the efficiency of a device is also affected by many other factors, such as device defects, and a theoretical efficiency (23%) has not been achieved.^[5] Optimization of these factors and the morphology of the active layer in particular to improve the overall device efficiency has received the most extensive attention in recent years.^[6] The efforts have led to the achievement of bench-mark efficiencies above 13.1%.^[7] The creation of the nanostructures has been largely achieved through tuning the solvent properties (e.g., using mixtures of solvents) and using additives,^[4,6] however, many of the solvents and additives are toxic. Supramolecular gels consisting of nanofibrous networks have received significant interest for organic electronics applications. The advantages of gels include the use of greener solvents such as alcohols, and a great flexibility in tuning the nanofibrous structure.^[8] However, they have been largely studied for energy transfer (in bulk gels), with limited device applications.^[3b,9] Encouragingly, a recent work demonstrated that a high photoconductivity could be achieved with a supramolecular gel system, which suggests a promising future for this class of materials for device applications.^[10]

Apart from device defects and improper morphology of the active layer, self-quenching of chromophores is another important factor that reduces the efficiency of an organic electronic

[a] Dr. J.-Y. Chen, Dr. A. Gupta, Dr. J.-L. Li
Institute for Frontier Materials,
Deakin University, Geelong, Victoria (Australia)
E-mail: akhilgk15@gmail.com
jli@deakin.edu.au

[b] G. Kadam, Prof. D. S. Dalal
Department of Organic Chemistry, School of Chemical Sciences
North Maharashtra University, Jalgaon 425001 Maharashtra (India)

[c] Anuradha
School of Science, RMIT University, Melbourne (Australia)

[d] Prof. S. V. Bhosale
Department of Chemistry, Goa University
Taleigao Plateau, Goa 403206 (India)
E-mail: svbhosale@unigoa.ac.in

[e] Dr. F. Zheng, Dr. C.-H. Zhou, Prof. B.-H. Jia
Centre for Micro-Photonics, Swinburne University of Technology
Hawthorn, Victoria 3122 (Australia)

Supporting information and the ORCID identification number(s) for the author(s) of this article can be found under:
<https://doi.org/10.1002/chem.201803158>.

device. For instance, a suitable molecular modification that modulates molecular packing reduced self-quenching and improved the external quantum efficiency of an OLED significantly.^[11] However, molecular modification is laborious and the packing of molecules is also affected by solvent and processing conditions. Using chromophores that are not subject to self-quenching is a promising approach to address the self-quenching problem. In recent years, chromophores with aggregation-induced emission (AIE) properties have attracted enormous research interest for various applications.^[12] In contrast to chromophores that self-quench upon aggregation, chromophores with AIE properties are not fluorescent when they are dissolved in solvents but give strong fluorescence when their molecules aggregate. There are several mechanisms for AIE, one of which is the restriction of molecular rotation.^[12] This property promises applications of chromophores in a number of emerging research areas such as biological imaging,^[13] OLEDs,^[14] luminescent solar concentrators (LSCs),^[15] and chemical sensing.^[16]

Despite the significant progress in the synthesis and applications of AIE chromophores, the use of supramolecular gels with AIE properties for charge transfer has not received much attention. To be a gelator for a solvent, a compound has to satisfy some basic requirements. Firstly, it should have a very limited solubility in a given solvent at ambient temperature; secondly, the non-dissolvable part must not precipitate from the solvent in the form of particulates. Only the formation of a strong solid network structure can lead to the formation of a self-standing gel.^[8a] Although increasing understanding of the molecular requirements for a gelator has been achieved in recent years,^[17] successful gelation is still hard to predict because the solvent properties significantly affect the gelling capacity of a gelator.^[18] In brief, the self-assembly of a gelator is enabled by some specific intermolecular noncovalent interactions (one or more types of forces such as hydrophobic interactions, hydrogen bonding, and π - π stacking).^[19] The properties of a solvent not only determine the solubility of a gelator, but also affect the intermolecular interactions of a gelator. Hence, a gelator works only for a few solvents. In this sense, design and synthesis of gelators is costly and laborious. Co-assembly with common gelators is a more convenient approach. It also reduces cost by using a smaller amount of target materials, which are expensive to produce in general. Moreover, the cores of AIE chromophores such as those based on tetraphenylethylene (TPE) are generally not planar (i.e., twisted),^[20] making it difficult for different AIE molecules to co-assemble. Hence, co-assembly on a backbone is an approach that could bring donor and acceptor chromophores close enough for charge transfer to occur.

In this work, supramolecular gels with AIE were prepared by co-assembling AIE chromophores 2,2',2'',2'''-(4',4'',4''',4''''-(ethene-1,1,2,2-tetrayl)tetrakis([1,1'-biphenyl]-4-carbonyl)tetrakis(azanediyl)tetrakis(N^1, N^5 -didodecylpentanediamide) (coded as S109) or (5Z,5'Z,5''Z,5'''E)-5,5',5'',5'''-(((ethene-1,1,2,2-tetrayl)tetrakis(benzene-4,1-diyl)tetrakis(thiophene-5,2-diyl)tetrakis(methanylylidene)tetrakis(4-methyl-1-octyl-2,6-dioxo-1,2,5,6-tetrahydropyridine-3-carbonitrile) (coded as TPE-CP4) with a non-

fluorescent gelator, *tert*-butyl 5-(octadecylamino)-2-(octadecyl-carbamoyl)-5-oxopentanoate (GluLC18). S109 and TPE-CP4 are based on a TPE core (electron-rich), which is well-known for its AIE properties.^[12,21] TPE-CP4 has electron-poor peripheral groups that can withdraw electrons from the TPE core. Hence, S109 and TPE-CP4 can be an electron donor and acceptor pair. GluLC18 is an amino acid derivative, having a combination of structural features such as long alkyl chains and amide groups, which help supramolecular assembly through van der Waals force, hydrophobic interactions, and hydrogen bonding. GluLC18 and molecules with similar structures have demonstrated excellent gelling capacity for various solvents.^[22] To facilitate co-assembly with GluLC18, S109 was designed with amide groups and long alkyl chains. TPE-CP4 also carries octyl chains as its peripheries. On a molar basis, the concentration of GluLC18 used for co-assembly in this study is a few orders of magnitude higher than those of S109 and TPE-CP4. Hence, the assembled structure of GluLC18 serves as a supramolecular backbone, similar to the protein complex of a natural light-harvesting system, enabling spatial attachment of the molecules of S109 or TPE-CP4 through noncovalent interactions.

It was observed that in tertiary gels composed of GluLC18, S109, and TPE-CP4, the fluorescence of S109 was efficiently quenched by TPE-CP4. However, fluorescence emission from TPE-CP4 was not observed. This phenomenon can be explained by a charge transfer mechanism. The highest occupied molecular orbital (HOMO) energy level of S109 estimated using photoelectron spectroscopy in air (PESA) is around -5.78 eV (Figure S1, Supporting Information). Its lowest unoccupied molecular orbital (LUMO) energy level calculated using the absorption onset is -3.15 eV (the optical band gap is 2.63 eV). The LUMO level of TPE-CP4 is -3.90 eV.^[23] These energy levels suggest that charge transfer from S109 (electron donor) to TPE-CP4 (electron acceptor) can occur as the electron can hop on very easily due to a large energy offset. This work demonstrates that charge transfer between an AIE electron donor and an AIE acceptor can be achieved via a simple supramolecular co-assembly approach.

The molecular structures of GluLC18, S109, and TPE-CP4 are shown in Figure 1.

Results and Discussion

Co-assembly of S109 and GluLC18

For gel formation, a compound should have a limited solubility in a solvent at ambient temperatures. S109 is barely soluble in dimethyl sulfoxide (DMSO) at room temperature. It is not fluorescent when it is dissolved at a high temperature (e.g., 110°C). Upon cooling the hot solution, it precipitated in the form of fluorescent aggregates due to AIE. The aggregates are composed of very thin and short fibers (Figure 2a). To form a gel, we adopted a co-assembly approach, using nonfluorescent GluLC18 as a co-gelator. The choice of DMSO as the solvent is also based on the known gelling capacity of GluLC18 in this solvent.^[22a] GluLC18 molecules self-assemble into spherulitic fibrous networks in DMSO, forming a gel when its concentration

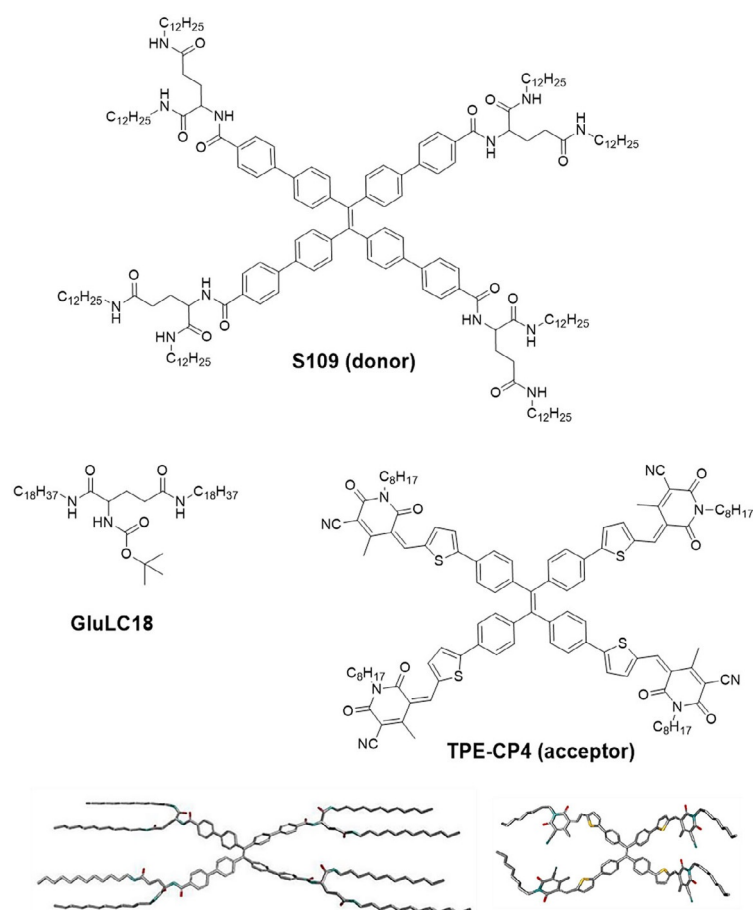


Figure 1. Molecular structures of newly designed donor S109, GluLC18, and acceptor molecule TPE-CP4. The three-dimensional structures of S109 (bottom left) and TPE-CP4 (bottom right) show that their aromatic cores are twisted.

is above 10 mM. Figure 2b shows a white-light microscopic image of GluLC18 fiber networks at a concentration of 13 mM, which was used to form binary and tertiary gels in this work.

The diameters of the spherulites range from 25 μm to above 100 μm . Fluorescent spherulitic fiber networks form in the binary gels with different loadings of S109 (Figure 2c–f), indicating co-assembly of the two components.

Upon increasing the concentration of S109, the size of the spherulites is progressively reduced and the number density of spherulites is increased, meaning that the nucleation of GluLC18 is promoted (Figure 2c–f). Real-time observation of fiber network formation showed that when a hot solution of GluLC18 (13 mM) in DMSO was cooled, fiber formation took place when the temperature was reduced (cooling rate 20 $^{\circ}\text{C}\text{min}^{-1}$) to ca. 45 $^{\circ}\text{C}$. In contrast, when S109 is present at a concentration of 10 μM , the temperature for fiber formation is ca. 55 $^{\circ}\text{C}$, indicating that S109 promotes fiber nucleation and growth.

The fiber network formation of molecular gels and many macromolecular gels is a nucleation and growth process.^[24] The primary nucleation rate determines the number of fiber network domains in a certain gel volume. According to 3D nucleation theory, the primary nucleation rate J can be expressed by Equations (1) and (2):^[24b]

$$J = f'[f]^{1/2} B \exp[-\Delta G^*/(kT)] \quad (1)$$

$$\Delta G^* = 16\pi\gamma_{cf}^3\Omega^2 / \{3(kT)^2[\Delta\mu/(kT)]^2\} \quad (2)$$

where ΔG^* is the nucleation energy barrier, B is the kink kinetics coefficient, f' and f ($f \leq 1$, $f > 0$) are factors describing the correlation between the substrates and the nucleation phase; k is the Boltzmann constant, T is temperature, Ω is the volume of the growth units, γ_{cf} denotes the interfacial free energy between the fibers and the fluid phase, $\Delta\mu$ denotes the chemical potential differ-

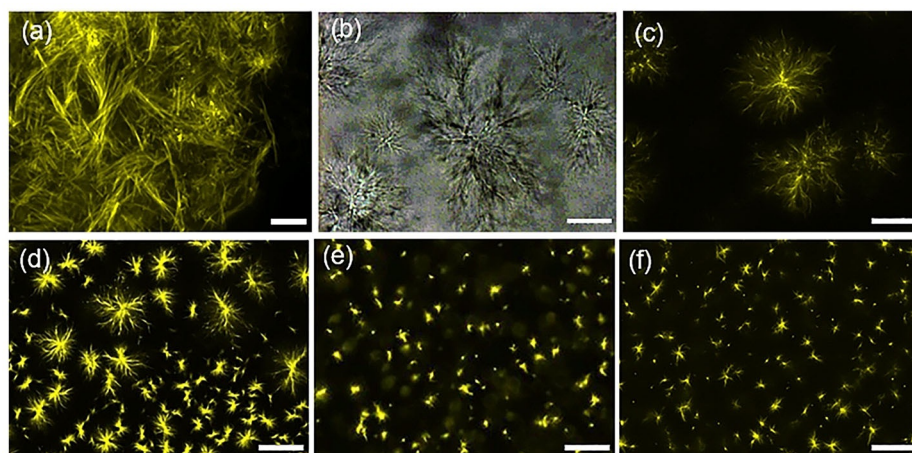


Figure 2. Microscopic and confocal images. a) Confocal image of fibrous aggregates of S109 formed in DMSO. b) Microscopic image of gel with only GluLC18 (13 mM), confocal images of binary gels with GluLC18 (13 mM) and S109 at c) 2.8 μM , d) 10 μM , e) 40 μM , and f) 100 μM . The scale bar in (a) represents 5 μm , and those in (b)–(f) represent 25 μm .

ence between gelator molecules in the fiber state and in the liquid.

In a certain solvent, when temperature and concentration of a gelator are fixed, the chemical potential $\Delta\mu$ is constant, and the nucleation rate is determined by the structure match between the substrate and nucleating phase. As shown in Figure 2, increasing S109 concentration leads to the formation of more domains with smaller sizes. S109 can interact with GluLC18 through noncovalent interactions including van der Waals forces, hydrophobic interactions between their long alkyl chains, and hydrogen bonding between their amide groups. Our recent work demonstrated that two molecular gelators with long alkyl chains could co-assemble to give gels with tunable structure and rheological properties.^[25] Compared with GluLC18, S109 has a bigger and hence more rigid molecular structure, together with higher hydrophobicity. This structural feature means that S109 can promote nucleation and growth of fibers in two ways. Firstly, the molecules of S109 have a higher tendency to adsorb on substrates such as dust particles. Secondly, the molecules of S109 are also easier to aggregate, especially when the concentration is high, to form nucleation centers. These two mechanisms reduce the nucleation energy barrier. When the S109 concentration is high enough (e.g., 1.2 mM), particles form together with tiny spherulitic fiber works (Figure S2, Supporting Information), which confirms the preferential self-aggregation of S109 molecules at higher supersaturations.

The XRD spectra of S109 and the binary aerogels are shown in Figure S3 (see the Supporting Information). S109 powders have a main peak at 20.5° , whereas the spectrum of the binary aerogel (GluLC 18: 13 mM, S109: 200 μM) is similar to that of plain GluLC18 with a main peak at 21.6° , indicating that the crystalline structure of the binary aerogels is dominated by

GluLC18. Hence, it is reasonable to assume that S109 is not embedded in gel fibers. The alkyl and amide functionalities of S109 facilitate strong interactions of its peripheral chains with GluLC18 through hydrophobic forces and hydrogen bonding, respectively. The drastic changes in the microstructure of GluLC18 fiber network induced by S109 (Figure 2b–f) also indicate that strong interactions exist between these two compounds. As a result, some (or all) of the peripheral chains of a S109 molecule should be integrated in fibers, leaving its aromatic TPE core on the fiber surface (Scheme S1, Supporting Information).

Fluorescence of co-assembled GluLC18 and S109 gels

The excitation spectra of S109 in the binary gels are given in Figure 3a. The main excitation peak shifts from 380 to 424 nm when the concentration of S109 increases from 2.8 to 200 μM , indicating the molecular packing of S109 is changed. At low concentrations of 2.8 and 10 μM , S109 in gel has two excitation peaks at 310 and 380 nm. At these S109 concentrations, the molar ratios of GluLC18 to S109 are 4600 and 1300, respectively, which means S109 molecules are only sparsely decorated on fibers and the chance for self-packing of the molecules on the fibers is low. When the S109 concentration is 40 μM (molar ratio of GluLC18 to S109 is 325) and above, redshift in the excitation spectrum occurs, which is more significant when the concentration of S109 is 200 μM . This indicates that S109 molecules may self-stack/aggregate on the fiber surface (Scheme S1, Supporting Information). A comparison with the excitation of pure S109 aggregates (Figure 3b) also indicates that the excitation of S109 in the binary gels (Figure 3a), especially at high concentrations, is redshifted. For example, at a concentration of 200 μM , the maximal excitation of pure S109

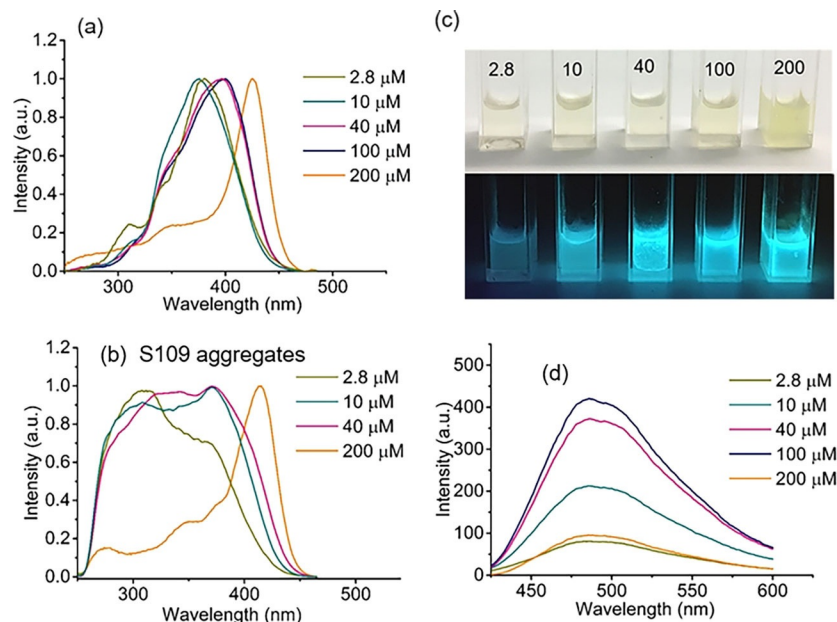


Figure 3. Spectroscopic characterization of S109 co-assembled with GluLC18, a) excitation of gels, b) excitation of S109 aggregates formed in DMSO, c) images of the GluLC18-S109 gels taken under room light (upper row) and a UV lamp with a wavelength of 365 nm (bottom row), and d) emission of gels. The emission wavelengths used to obtain the spectra in (a) and (b) were 500 and 480 nm, respectively, and the excitation wavelength used to obtain the spectra in (d) was 400 nm.

is 414 nm, which shifts to 422 nm for the binary gel. The red-shift of the excitation wavelength indicates that the π - π stacking is more off-facial (i.e., J-aggregates),^[26] which could be due to disturbance of GluLC18 on the molecular packing of S109. In the co-assembled gels, S109 gives strong fluorescence even at the low concentration of 2.8 μM . The four arms of S109 can interact with different molecules of GluLC18 so that the rotation of S109 molecules is restricted, similar to aggregation-restricted rotation, leading to fluorescence emission (Figure 3c).

The potential interactions between GluLC18 and S109 are also indicated by rheological studies. The storage moduli G' , a measure of elasticity of a gel, is determined by both the structure of its fiber network and the fiber mass. For a gel with a spherulitic fiber structure, its G' is generally compromised when the sizes of the spherulites are reduced due to promoted nucleation, if fiber mass is fixed.^[8a,24c,27] S109 at 2.8 μM significantly reduces the size of spherulites, which is expected to lead to significant reduction in G' . However, no observable changes in G' were caused by S109. The G' of the gel either in the presence and absence of S109 is ca. 2950 Pa. Because the addition of S109 at this concentration (0.0075 mg mL^{-1}) negligibly changes fiber mass (the concentration of GluLC 18 is 10 mg mL^{-1}), the interactions of the four arms of S109 with GluLC18 may compensate the negative effect of size reduction on G' . The interactions led to an observable increase in G' when the S109 concentration is high enough, for example 200 μM (0.5 mg mL^{-1}). The G' of the gel at this S109 concentration is 4000 Pa, which is 1000 Pa higher than the gel formed by GluLC18 only. However, S109 at this concentration contributes to a 5% increase in fiber mass. To understand the effect of fiber mass increase on G' , the concentration of pure GluLC18 gel was increased to 10.5 mg mL^{-1} , which leads to a G' of 3600 Pa, still lower than that of the binary gel.

It was also observed that, with an increase in the concentration of S109 to 100 μM , the gel fluorescence was enhanced (Figure 3d). When its concentration was increased to 200 μM , fluorescence intensity was greatly reduced. The excitation wavelength used to obtain the fluorescence spectra in Figure 3d was fixed at 400 nm. The gels were also excited at their wavelengths of maximal absorption according to Figure 3a. The emission intensities (Figure S4, see the Supporting Information) were observed to follow a trend similar to that in Figure 3d.

The significant reduction in fluorescence at high S109 concentration of 200 μM may be partially due to a significant increase in the turbidity of the gel that reduces its light transmission (Figure 3c). The fluorescence emission of a chromophore is also dependent on its quantum yield. It has been a challenge to quantify the quantum yield of a chromophore in a wet gel state, due to light reflection by gel fibers. The quantum yields of powders (aerogels) can be obtained using integrating spheres. However, removing the solvent from a gel may influence the molecular packing of gel fibers, which affects both the absorbance and fluorescence of the chromophore. Therefore, we simply estimate the quantum yields of all the gels relative to the gel at the lowest S109 concentration of

2.8 μM , based on their light absorbance and fluorescence. Assuming the quantum yield of S109 at 2.8 μM is one unit, the quantum yield Q at other concentrations can be calculated from $Q = I/I_{2.8} \times (OD_{2.8}/OD)$, where I and OD are fluorescence density and optical density, respectively, which are the area below the fluorescence and light absorption spectra. The UV/Vis absorption spectra of the gels are given in Figure S5 (see the Supporting Information). This calculation is based on the assumption that the fractions of reflected light are the same for all the gels. The quantum yields of the gels at S109 concentrations of 10, 40, 100, and 200 μM are, respectively, 1.02, 2.87, 1.70, and 0.33 times the quantum yield of the gel with 2.8 μM S109. The highest quantum yield was obtained at the S109 concentration of 40 μM . The variation of quantum yields is interesting. It was reported that the quantum yield of a TPE-based AIE molecule was significantly enhanced (compared to its powders) when it was fixed in a metal-organic framework due to restricted molecular flexibility.^[28] The fiber network of this work has a similar effect on the molecular flexibility of S109. When the concentration of S109 is low, the fiber network has a greater effect on restricting its molecular rotation, whereas when the concentration of S109 is high enough (e.g., 200 μM), self-packing may occur, reducing the influence of fiber network. It has been reported that the molecular packing of an AIE chromophore also affects its emission properties.^[29] Hence, the fluorescence properties of an AIE chromophore in a gel fiber network is a very complex and an interesting subject of investigation. Based on the above observations, the gel with a S109 concentration of 40 μM , which has a fluorescence intensity only slightly lower than that of the gel containing 100 μM of S109, was used for charge transfer studies.

Co-assembly of GluLC18 and TPE-CP4

Co-assembly of TPE-CP4 with GluLC18 is also evident from the color change and fluorescence of the gels, as well as confocal images. A solution of TPE-CP4 in DMSO (without GluLC18) is red (the top left cuvette in Figure 4a), which is not fluorescent under a UV light (the bottom left cuvette in Figure 4a). Whereas, its gels with GluLC18 are yellow, giving green fluorescence under a UV light. The emission of TPE-CP4 in a gel state would be due to restricted rotation of its TPE core. The fluorescence spectra in Figure 4b show that, with an increase in the concentration of TPE-CP4 to 27 μM , the fluorescence of the gel is enhanced. A further increase in its concentration reduces the gel fluorescence. At a concentration of 81 μM , the fluorescence of the gel almost disappears. The self-quenching of TPE-CP4 at high concentrations shall be attributable to intramolecular and intermolecular charge transfer. The molecule of TPE-CP4 has both electron-rich (the TPE core) and electron-poor (the peripheral parts) moieties, which makes it possible for intramolecular charge transfer, leading to self-quenching. This may explain the weaker fluorescence of the GluLC18-TPE-CP4 gels, compared with the GluLC18-S109 gels. When the concentration of TPE-CP4 in the gel is increased to a certain level, self-stacking of TPE-CP4 takes place, which facilitates intermolecular charge transfer. Self-stacking of TPE-CP4 at high concentra-

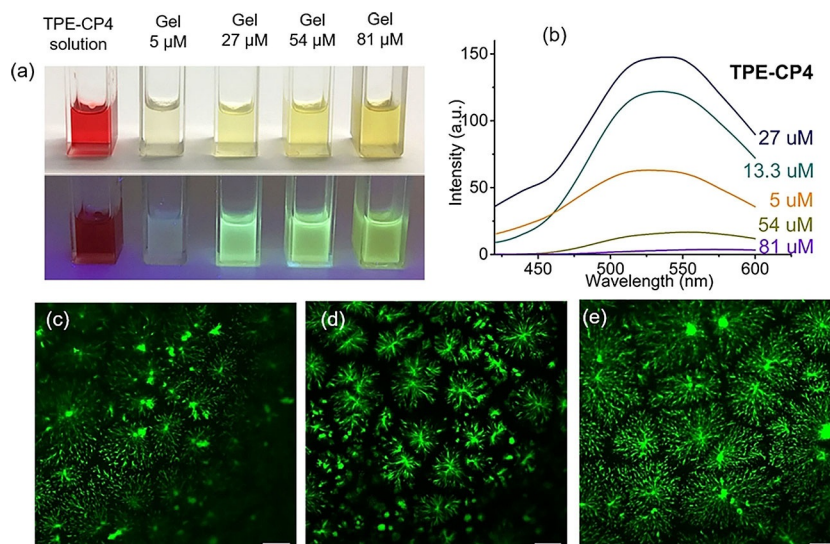


Figure 4. Fluorescence and microscopic characterization of GluLC18-TPE-CP4 gels. a) Images of samples taken under room light (upper row) and a UV lamp with a wavelength of 365 nm (lower row). b) Fluorescence spectra, and confocal microscopic images of gels at TPE-CP4 concentrations of c) 5, d) 13.3, and e) 27 μM , respectively. The concentration of TPE-CP4 in the solution (the left cuvette of (a)) was 27 μM . The scale bars in (c)–(e) represent 25 μm . The excitation wavelength used to obtain the spectra in (b) was 400 nm.

tions of 54 and 81 μM is evident from the confocal images shown in Figure S6 (see the Supporting Information). The aggregation of TPE-CP4 on GluLC18 fibers makes the fibrous structure non-discernible. S109 powders have strong fluorescence, whereas powders of TPE-CP4 are not fluorescent (the middle image of Figure 5 a), although they have the same TPE core. This indicates self-packing of TPE-CP4 molecules induces self-quenching due to its specific donor–acceptor structure. It was observed that with an increase in its concentration, the fluorescence of TPE-CP4 in the gel decays faster and the lifetime was progressively reduced from 1.38 to 1.16 ns when its concentration was varied from 5 to 81 μM (Figure S7, Supporting Information). It has been reported that the intramolecular charge transfer of a chromophore with a donor–acceptor molecular structure is affected by the twisting degree of its molecule.^[30] Co-assembly with GluLC18 may affect the twisting degree of TPE-CP4 molecules to modulate its fluorescence emission. This is a subject of interest and worth a detailed study.

Confocal microscopic characterization shows that the networks of the GluLC18-TPE-CP4 gels are fluorescent and remain spherulitic (Figure 4 c–e). In contrast to S109, TPE-CP4 does not cause a significant change to the size of the spherulites, thus indicating that it does not have a big influence on the nucleation of GluLC18. The side groups of TPE-CP4, which contain shorter alkyl chains and do not have amide groups, are not so similar to the structure of GluLC18. Hence, its interaction with GluLC18 is weaker, compared with S109.

Charge transfer using co-assembled AIE gels

Without the assistance of GluLC18, S109, and TPE-CP4 cannot co-assemble to form a gel. It was observed that when a hot solution of these two compounds in DMSO was cooled, S109

self-aggregated (the right image of Figure 5 a). In the presence of GluLC18, co-assembled tertiary gels form. It is interesting to

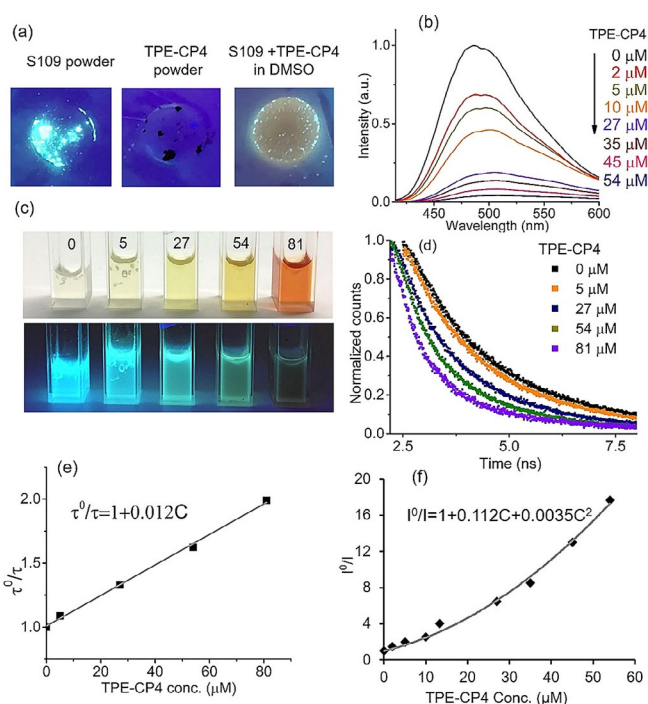


Figure 5. Charge transfer from S109 to TPE-CP4. a) Images of S109 powder, TPE-CP4 powder and a mixture of them in DMSO taken under irradiation with a UV lamp. b) Fluorescence quenching of S109 by TPE-CP4 in co-assembled gels. c) Images of gels under room light and a UV lamp with a wavelength of 365 nm. d) The effects of TPE-CP4 on fluorescence decay of S109. e) Correlation of lifetime change with TPE-CP4 concentration, and f) Stern–Volmer plot of the charge-transfer system. The concentrations of GluLC18 and S109 were fixed at 13 μM and 40 μM , respectively. The excitation wavelength used to obtain the spectra in (b) was 400 nm.

observe that the fluorescence of S109 (40 μM) was progressively quenched with the increase in TPE-CP4 concentration (Figure 5b). More than 90% of its fluorescence was quenched when the concentration of TPE-CP4 was 54 μM . Complete quenching was observed when 81 μM of TPE-CP4 was present. This concentration is over twice the concentration of S109 (40 μM).

Fluorescence quenching generally occurs through fluorescence energy transfer (FRET) or charge transfer. The occurrence of FRET needs a donor and acceptor molecule to locate within a distance of 10 nm and a significant overlap between the donor emission and acceptor absorption spectra. However, this is not the case for S109 and TPE-CP4, which showed negligible overlap of their spectra (Figure S8, Supporting Information). Compared to FRET, charge transfer requires closer localization (< 10 Angstroms) of the donor and acceptor molecules.^[31] FRET leads to quenching of the donor fluorescence and emission of acceptor fluorescence when the donor is excited, whereas charge transfer generally leads to quenching of a donor without the emission of an acceptor, as the acceptor molecules are converted into radical anions.^[31] Based on their HOMO and LUMO energy values, S109 and TPE-CP4 are a perfect pair of electron-donor and -acceptor.

Fluorescence quenching is visually evident from the gels under UV light irradiation (the bottom images of Figure 5c). When the concentration of TPE-CP4 is 81 μM , the gel fluorescence is barely observable. Under room light, the gel is red (the top right cuvette of Figure 5c). The color is lighter than the color of the 27 μM TPE-CP4 solution (Figure 4a), which means the concentration of TPE-CP4 is excessive and some of its molecules are dissolved in the solvent phase of the gel (with a dissolved concentration less than 27 μM). When S109 is not present, at this concentration (81 μM), most TPE-CP4 molecules are attached to GluLC18 fibers, as indicated by the yellow color (the top right cuvette in Figure 4a). Hence, it can be concluded that S109 competes with TPE-CP4 for co-assembly with GluLC18. Due to its longer alkyl chains and amide functionalities, S109 has stronger interactions with GluLC18. Confocal microscopic observation indicates that TPE-CP4 does not have a significant effect on the microscopic gel fiber networks of GluLC18-S109 gels (Figure S9, Supporting Information). The sizes of the spherulites in the absence and presence of TPE-CP4 are similar, which means GluLC18 preferentially co-assemble with S109 and TPE-CP4 does not have a clear effect on the primary nucleation and fiber growth of GluLC18 and S109. The alkyl chains of GluLC18 can facilitate its interactions with TPE-CP4. Hydrogen bonds may also form between the oxygen atoms of TPE-CP4 and the amide groups of the gelator. TPE-CP4 could interact with GluLC18 molecules that are not associated with S109. When the fibers of GluLC18 are completely occupied, a further increase in TPE-CP4 would lead to the presence of unlinked (free) TPE-CP4 molecules. As discussed earlier, GluLC18 at a concentration of 13 mM can co-assemble with S109 at a concentration of 200 μM , at least when TPE-CP4 is not present. In the tertiary gels, the concentration of S109 is fixed at 40 μM . Hence, the GluLC18 fibers are not saturated with S109 and TPE-CP4 can attach to the fibers.

Figure 5d shows that the presence of TPE-CP4 accelerates the fluorescence decay of S109. There are two types of quenching, one is dynamic (collision) quenching affected by the diffusion of the quencher (or both quencher and donor), and the second is static quenching caused by complex formation between a donor and quencher. A linear fit of I^0/I against the quencher concentration C in terms of the Stern–Volmer equation [Eq. (3)] is generally obtained for dynamic quenching.^[32]

$$I^0/I = 1 + K_D C \quad (3)$$

where I^0 and I are the fluorescence intensity of a donor chromophore in the absence and presence of an acceptor, respectively, K_D is dynamic quenching constant and $K_D = k_q \tau_0$, in which τ_0 is the lifetime of donor in the absence of an acceptor, and k_q is bimolecular quenching constant. The value of τ_0 obtained by fitting the fluorescence decay curve (0 μM , Figure 5d) with an exponential decay function is 2.21 ns. The lifetime values obtained at the TPE-CP4 concentrations of 5, 27, 54, and 81 μM are 2.03, 1.66, 1.36, and 1.11 ns, respectively. Dynamic quenching also induces changes in the fluorescence lifetime of a donor, depending on the concentration of the quencher, as given by Equation (4):

$$\tau^0/\tau = 1 + K_D C \quad (4)$$

An important characteristic of static quenching is that it does not affect the lifetime of a donor. It was observed that the lifetime of S109 progressively decreased with an increase in TPE-CP4 concentration (Figure 5d) and a linear fit between τ^0/τ and quencher concentration was obtained (Figure 5e), indicating that dynamic quenching was involved. However, Figure 5f shows that a linear fit between I^0/I and the concentration of TPE-CP4 [Eq. (3)] was not obtained. The curve shows an upward curvature, concave to the Y axis. This type of curve indicates quenching of S109 is contributed by both dynamic and static processes.^[31] In such a case, I^0/I is generally a second-order function of quencher concentration, as given by Equation (5):

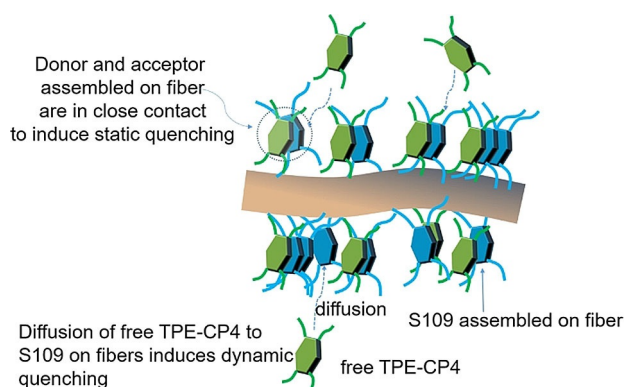
$$I^0/I = 1 + (K_S + K_D) \times C + K_S K_D \times C^2 \quad (5)$$

where K_S is the static quenching constant.

According to Equation (4), the dynamic quenching constant K_D is given by the slope of the linear fitting for $\tau^0/\tau \approx C$ (Figure 5e), which is 0.012 μM^{-1} (or $1.2 \times 10^4 \text{M}^{-1}$). This results in a bimolecular constant k_q of $5.45 \times 10^{12} \text{M}^{-1} \text{s}^{-1}$. Dynamic quenching generally has a k_q close to $1.0 \times 10^{10} \text{M}^{-1} \text{s}^{-1}$. A higher value indicates that some type of binding interactions exist between the donor and quencher.^[31] By fitting the quenching data to Equation (5) (Figure 5f), the static quenching constant K_S obtained from the first- and second-order coefficient is 0.1 and 0.29 μM^{-1} , respectively. Although slightly different, both values are an order of magnitude higher than the dynamic quenching constant, which indicates the static process plays a more significant role in quenching.

The presence of both dynamic and static quenching is feasible for the gels of this work. As both S109 and TPE-CP4 can co-assemble with GluLC18, the molecules of these two compounds could locate closely or even form complexes on the surface of GluLC18 fiber to facilitate static quenching. In addition, due to the weaker interactions between TPE-CP4 and GluLC18 and the higher solubility of TPE-CP4 (> 27 mM) in the solvent DMSO, some TPE-CP4 molecules may exist in the solvent phase of the gel, contributing to dynamic quenching of S109. With an increase of TPE-CP4 concentration, the amount of free TPE-CP4 molecules increases and dynamic quenching plays a more important role. As discussed earlier, the presence of free TPE-CP4 is evident when its concentration is $81 \mu\text{M}$. At this concentration, the fluorescence of S109 is almost completely quenched, with the value of $\rho//I$ equal to 702. As the fluorescence of the gel at this TPE-CP4 concentration is very low, a slight variation of fluorescence intensity has a drastic effect on the $\rho//I$ value; hence, it was not involved in the fitting in Figure 5 f. It is worth mentioning that, although free S109 molecules also exist in the gel solvent, any charge transfer that may happen from the free S109 molecules to the free TPE-CP4 molecules does not contribute to the fluorescence quenching of S109, as S109 is not fluorescent when it is dissolved in a solvent.

According to the above characterizations and analysis, the charge-transfer-induced fluorescence quenching of S109 by TPE-CP4 is schematically illustrated in Scheme 1. As S109 has a stronger affinity to GluLC18, its molecules co-assemble with those of GluLC18 through their alkyl chains. The aromatic parts of S109 are exposed on the fiber surface. TPE-CP4 molecules can attach to the fiber surface also through noncovalent interactions. The assembly of these two compounds on fibers facilitates their binding interactions between their aromatic parts. These close interactions are hard to achieve if fibers of



Scheme 1. Illustration of charge transfer from S109 to TPE-CP4. The fluorescence of S109 molecules attached to GluLC18 fibers is quenched by TPE-CP4 through a combination of static and dynamic processes. Static quenching takes place on S109 and TPE-CP4 assembled on gel fibers, and dynamic quenching happens when TPE-CP4 molecules dissolved in the solvent diffuse to S109 molecules on fibers. A S109 and TPE-CP4 could be associated with multiple fibers, which restricts their molecular rotations.

GluLC18 are not present, as they tend to self-assemble because of their twisted molecular structures (Figure 1). The self-assembly/aggregation of S109 molecules in DMSO has been clearly demonstrated (the right image of Figure 5 a). The free TPE-CP4 molecules dissolved in the solvent withdraw electrons from S109 through diffusion-controlled collision.

SEM characterizations were performed to understand the influence of TPE-CP4 on the nanoscale structure of the GluLC18-S109 gels. Although S109 affects nucleation and growth of GluLC18 fiber networks (Figure 2 b–f), the co-assembled fibers have a similar nanoscale structure (Figure 6 a and b). However, the addition of TPE-CP4 led to formation of more flat fibers, which is more evident when its concentration is higher (Fig-

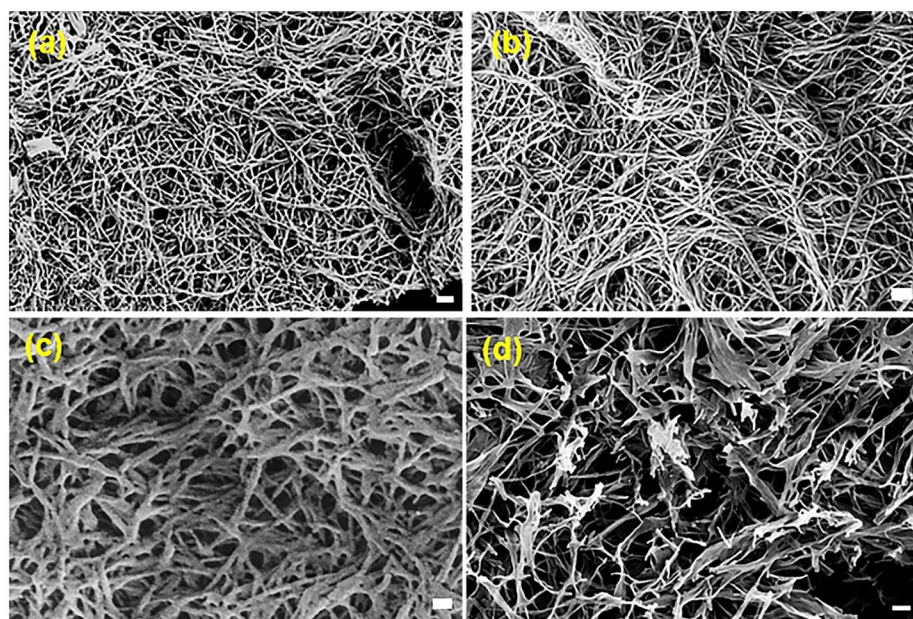


Figure 6. SEM images of aerogels. a) GluLC18 gel, b) binary gel of GluLC18 and S109, and tertiary gels with c) $0.4 \mu\text{M}$ TPE-CP4 and d) $2 \mu\text{M}$ TPE-CP4. The scale bar represents 200 nm. The concentrations of GluLC18 and S109 were fixed at 13 mM and $2.8 \mu\text{M}$, respectively.

ure 6d). This may also support its interfacial adsorption on fibers.

Conclusions

An electron-donating chromophore (S109) and an electron-accepting chromophore (TPE-CP4) based on TPE were designed and synthesized. A non-chromophoric gelator GluLC18 helped the co-assembly of these two compounds. These chromophores show AIE properties when they individually co-assemble with GluLC18, indicating that their molecular rotation is restricted in gels. The fluorescence of the donor can be efficiently quenched by the acceptor due to charge transfer when both of them are present in the gel. A complete quenching was observed when the molar ratio of the acceptor to donor is over two. The fluorescence quenching is a combination of dynamic and static processes, since the gel is a two-component system in which the donor and acceptor are present both in the solid fiber phase and in the solvent phase. The static charge transfer takes place between the donor and acceptor molecules assembled on fibers and the dynamic process happens between the free acceptor molecules in solvent and the donor molecules on fibers. The fibers of the nonfluorescent gelator GluLC18 serve as backbones for the formation of donor-acceptor complexes, similar to the protein-assisted charge-transfer system in nature. The results of this work demonstrate that supramolecular assembly can be an effective approach for charge transfer between an AIE donor and acceptor.

Experimental Section

Materials

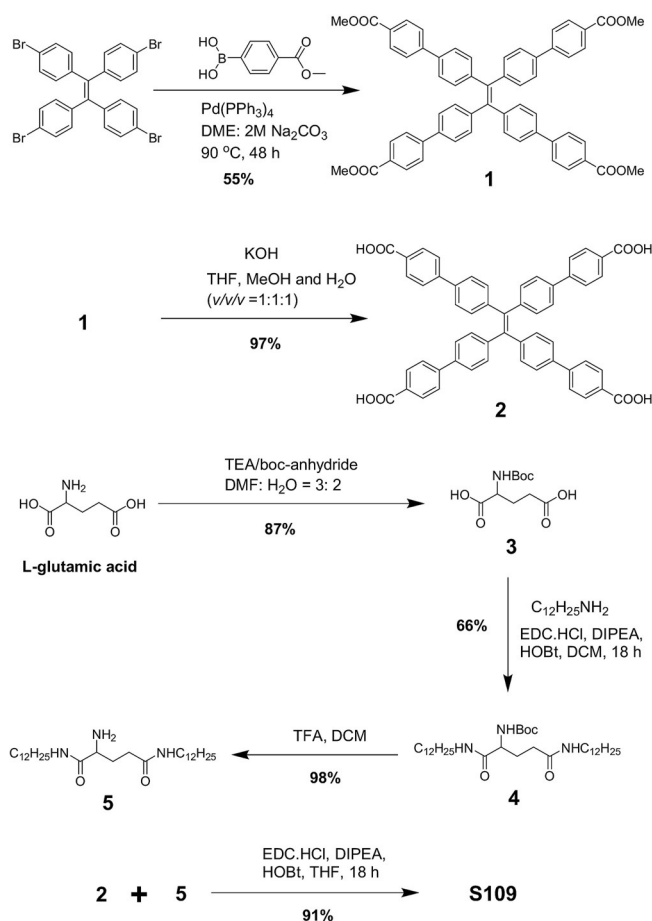
All the reactions were carried out under a nitrogen atmosphere, unless otherwise stated. Solvents used for various reactions were dried using a commercial solvent purification/drying system. Solvent used for extractions and column purifications and all other reagents were used as supplied by commercial vendors without further purification or drying. The synthesis of TPE-CP4 has been reported previously.^[23] GluLC18 was also synthesized as per the reported literature.^[22a]

Synthetic strategy

The target material S109 was prepared by reacting 4',A''',A''''',A''''''-(ethene-1,1,2,2-tetrayl)tetrakis([1,1'-biphenyl]-4-carboxylic acid) (intermediate **2**) and 2-amino-*N*1,*N*5-didodecylpentanediamide (intermediate **5**) in the presence of *N*-(3-dimethylaminopropyl)-*N'*-ethylcarbodiimide hydrochloride and *N,N*-diisopropylethylamine using a catalytic amount of 1-hydroxybenzotriazole. The intermediates **2** and **5** were synthesized by using reported procedures but with slight modifications.^[33] The synthetic strategy for S109 and related intermediates is represented in Scheme 2. Details of synthesis are given in the Supporting Information.

Characterization

Thin-layer chromatography (TLC): TLC was performed using 0.25 mm thick plates pre-coated with Merck Kieselgel 60 F254 silica gel, and visualized using UV light (254 and 365 nm). Petrole-



Scheme 2. Synthetic strategy used to generate S109.

um spirits with a boiling point range of 40–60 °C was used wherever indicated. Column chromatography was performed on either 40–60 or 20–40 μm silica gel. ^1H NMR spectra were recorded at 300, 400, or 500 MHz, as indicated. The following abbreviations are used to denote multiplicities: s=singlet, d=doublet, t=triplet, q=quartet, m=multiplet, br=broad, dd=doublet of doublets, and dt=doublet of triplets. ^{13}C NMR spectra were recorded at 75 or 101 MHz, as indicated. ^1H and ^{13}C chemical shifts were calibrated using residual non-deuterated solvent as an internal reference and are reported in parts per million (δ) relative to tetramethylsilane ($\delta=0$ ppm).

Determination of the HOMO and the LUMO energy levels of S109: Estimation of the HOMO and the LUMO energy levels of S109 were based on a combination of photoelectron spectroscopy in air (PESA) and UV/Vis spectroscopy.^[34] A Riken Keiki AC-2 PESA spectrometer with a power number of 0.5 was used. Samples for PESA were prepared on ITO cleaned glass substrates and were run using a power setting of 10 nW (incident photon energy range = -4.2 to -6.2 eV).

Gel formation and thin-film formation: Gels were prepared by dissolving the gelators (GluLC18 and S109) with or without TPE-CP4 at 110 °C in glass vials. Self-supporting gels formed when the hot solutions were cooled. Thin-gel films (300 μm) were formed in self-made glass cells. A Linkam heating and cooling stage (THMS600) was used to melt the gels at 110 °C and cooled to 25 °C at a cooling rate of 20 °C min^{-1} . In this manner, all the gel films were formed under the same thermal conditions. The gel films

were used to obtain the gel networks with optical and confocal microscopy (Leica confocal microscope, excitation 405 nm).

Preparation of aerogels and X-ray diffraction (XRD): Aerogels were obtained by extracting the solvent DMSO from gels with a supercritical fluid extraction system (SFE, Applied Separations). The aerogels were studied with XRD (PANalytical X'pert Pro) for crystal-line study using a $\text{Cu}_{\text{K}\alpha}$ radiation source operated at 40 kV. The samples were scanned with a step angle of 0.013° .

Characterization of fluorescence emission: A Hitachi fluorescence spectrometer (F4500) was used to characterize the fluorescence and excitation spectra of gels. For charge transfer, a concentrated solution (1 mm) of acceptor was prepared and aliquots of the solution were added into hot solutions (3.0 mL) of S109 and GluLC18 in DMSO. The total volumes of the mixture were adjusted to the same using DMSO. After well mixing, the solutions were cooled naturally to RT and spectra were obtained after one day of gel setting. The excitation wavelength was set at 400 nm.

Characterization of fluorescence lifetime decay: The time-correlated single-photon counting (TCSPC) technique was used to characterize time-resolved fluorescence decay of gels without and with the acceptor. A 405 nm pulsed laser beam (40 ps width) with a repetition rate of 2 MHz was generated by a picosecond pulsed diode laser driver (PDL 800-D, PICO QUANT Inc.) and used as the excitation light. The collected fluorescence signals (from the whole spectra) of the samples were transmitted through an optical fiber to a TCSPC module (PicoHarp 300, PICO QUANT Inc.) for single-photon counting analysis.

Rheological characterization: An Advanced Rheological Expansion System (ARES-2, TA) was used to characterize the storage moduli of the gels. The sol-gel process was performed in situ between two parallel plates with a gap of 0.5 mm. The amplitude of the oscillation was controlled to obtain a strain of 0.02% and the oscillation frequency was set at 0.1 Hz. The temperature ramp rate was $20^\circ\text{C min}^{-1}$.^[25,35]

Acknowledgements

This work was supported by the Australian Research Council (ARC) through a Future Fellowship project (FT130100057). J.-L.L. also acknowledges the ARC for support through an Industrial Transformation Research Hub for a Future Fibre Industry (IH140100018). A.G. acknowledges Deakin University for support through an Alfred Deakin Postdoctoral Research Fellowship. S.V.B. acknowledges the University Grant Commission (UGC)-Faculty Research Program (India) for providing financial support.

Conflict of interest

The authors declare no conflict of interest.

Keywords: aggregation-induced emission • charge transfer • gels • self-assembly • supramolecular chemistry

[1] H. J. Wörner, C. A. Arrell, N. Banerji, A. Cannizzo, M. Chergui, A. K. Das, P. Hamm, U. Keller, P. M. Kraus, E. Liberatore, P. Lopez-Tarifa, M. Lucchini, M. Meuwly, C. Milne, J.-E. Moser, U. Rothlisberger, G. Smolentsev, J. Teuscher, J. A. van Bokhoven, O. Wenger, *Struct. Dyn.* **2017**, *4*, 061508.

- [2] a) Y. Liu, J. Jin, H. Deng, K. Li, Y. Zheng, C. Yu, Y. Zhou, *Angew. Chem. Int. Ed.* **2016**, *55*, 7952–7957; *Angew. Chem.* **2016**, *128*, 8084–8089; b) C. Reinbothe, N. Lebedev, S. Reinbothe, *Nature* **1999**, *397*, 80–84.
- [3] a) K. Sakakibara, P. Chithra, B. Das, T. Mori, M. Akada, J. Labuta, T. Tsuruoka, S. Maji, S. Furumi, L. K. Shrestha, J. P. Hill, S. Acharya, K. Ariga, A. Ajayaghosh, *J. Am. Chem. Soc.* **2014**, *136*, 8548–8551; b) S. S. Babu, V. K. Praveen, A. Ajayaghosh, *Chem. Rev.* **2014**, *114*, 1973–2129; c) A. Ajayaghosh, V. K. Praveen, C. Vijayakumar, *Chem. Soc. Rev.* **2008**, *37*, 109–122.
- [4] a) J. Lee, D. H. Sin, B. Moon, J. Shin, H. G. Kim, M. Kim, K. Cho, *Energy Environ. Sci.* **2017**, *10*, 247–257; b) M. Kim, J. H. Park, J. H. Kim, J. H. Sung, S. B. Jo, M. H. Jo, K. Cho, *Adv. Energy Mater.* **2015**, *5*, 1401317.
- [5] T. Kirchartz, K. Taretto, U. Rau, *J. Phys. Chem. C* **2009**, *113*, 17958–17966.
- [6] H. Lee, C. Park, D. H. Sin, J. H. Park, K. Cho, *Adv. Mater.* **2018**, *30*, 1800453.
- [7] a) W. Zhao, S. Li, H. Yao, S. Zhang, Y. Zhang, B. Yang, J. Hou, *J. Am. Chem. Soc.* **2017**, *139*, 7148–7151; b) X. Xu, T. Yu, Z. Bi, W. Ma, Y. Li, Q. Peng, *Adv. Mater.* **2018**, *30*, 1703973.
- [8] a) J. L. Li, X. Y. Liu, *Adv. Funct. Mater.* **2010**, *20*, 3196–3216; b) J. Y. Chen, Z. Komeily-Nia, L. P. Fan, Z. Y. Li, B. Yuan, B. Tang, J. L. Li, *J. Colloid Interface Sci.* **2018**, *526*, 356–365.
- [9] A. Del Guerzo, A. G. L. Olive, J. Reichwagen, H. Hopf, J. P. Desvergne, *J. Am. Chem. Soc.* **2005**, *127*, 17984–17985.
- [10] V. S. Nair, R. D. Mukhopadhyay, A. Saeki, S. Seki, A. Ajayaghosh, *Sci. Adv.* **2016**, *2*, e1600142.
- [11] H. Z. Xie, M. W. Liu, O. Y. Wang, X. H. Zhang, C. S. Lee, L. S. Hung, S. T. Lee, P. F. Teng, H. L. Kwong, H. Zheng, C. M. Che, *Adv. Mater.* **2001**, *13*, 1245–1248.
- [12] J. Mei, Y. Hong, J. W. Y. Lam, A. Qin, Y. Tang, B. Z. Tang, *Adv. Mater.* **2014**, *26*, 5429–5479.
- [13] J. Chen, H. Jiang, H. Zhou, Z. Hu, N. Niu, S. A. Shahzad, C. Yu, *Chem. Commun.* **2017**, *53*, 2398–2401.
- [14] Z. Zhao, J. W. Y. Lam, B. Z. Tang, *J. Mater. Chem.* **2012**, *22*, 23726–23740.
- [15] J. L. Banal, J. M. White, K. P. Ghiggino, W. W. H. Wong, *Sci. Rep.* **2014**, *4*, 4635.
- [16] R. Zhang, C.-J. Zhang, G. Feng, F. Hu, J. Wang, B. Liu, *Anal. Chem.* **2016**, *88*, 9111–9117.
- [17] R. G. Weiss, *J. Am. Chem. Soc.* **2014**, *136*, 7519–7530.
- [18] a) S. Wu, J. Gao, T. J. Emge, M. A. Rogers, *Soft Matter* **2013**, *9*, 5942–5950; b) Y. Lan, M. G. Corradini, R. G. Weiss, S. R. Raghavan, M. A. Rogers, *Chem. Soc. Rev.* **2015**, *44*, 6035–6058.
- [19] P. Terech, R. G. Weiss, *Chem. Rev.* **1997**, *97*, 3133–3159.
- [20] Y. Liu, C. Mu, K. Jiang, J. Zhao, Y. Li, L. Zhang, Z. Li, J. Y. L. Lai, H. Hu, T. Ma, R. Hu, D. Yu, X. Huang, B. Z. Tang, H. Yan, *Adv. Mater.* **2015**, *27*, 1015–1020.
- [21] X. Xue, Y. Zhao, L. Dai, X. Zhang, X. Hao, C. Zhang, S. Huo, J. Liu, C. Liu, A. Kumar, W. Chen, G. Zou, X.-J. Liang, *Adv. Mater.* **2014**, *26*, 712–717.
- [22] a) Y. Li, T. Wang, M. Liu, *Soft Matter* **2007**, *3*, 1312–1317; b) J. L. Li, B. Yuan, X. Y. Liu, R. Y. Wang, X. G. Wang, *Soft Matter* **2013**, *9*, 435–442; c) J. L. Li, B. Yuan, X. Y. Liu, X. G. Wang, R. Y. Wang, *Cryst. Growth Des.* **2011**, *11*, 3227–3234.
- [23] A. Rananaware, A. Gupta, G. Kadam, D. D. La, A. Bilic, W. C. Xiang, R. A. Evans, S. V. Bhosale, *Mater. Chem. Front.* **2017**, *1*, 2511–2518.
- [24] a) J. L. Li, X. Y. Liu, C. S. Strom, J. Y. Xiong, *Adv. Mater.* **2006**, *18*, 2574–2579; b) X. Y. Liu, P. D. Sawant, W. B. Tan, I. B. M. Noor, C. Pramesti, B. H. Chen, *J. Am. Chem. Soc.* **2002**, *124*, 15055–15063; c) X. Huang, P. Terech, S. R. Raghavan, R. G. Weiss, *J. Am. Chem. Soc.* **2005**, *127*, 4336–4344; d) J. Y. Xiong, X. Y. Liu, J. L. Li, M. W. Vallon, *J. Phys. Chem. B* **2007**, *111*, 5558–5563; e) J. L. Li, X. Y. Liu, in *Soft Fibrillar Materials: Fabrication and Applications* (Eds.: X. Y. Liu, J. L. Li), Wiley-VCH, Weinheim, **2013**, pp. 163–181.
- [25] J. Y. Chen, B. Yuan, Z. Y. Li, B. Tang, A. Gupta, S. V. Bhosale, J. L. Li, *Langmuir* **2016**, *32*, 12175–12183.
- [26] a) A. Eisfeld, J. S. Briggs, *Chem. Phys.* **2006**, *324*, 376–384; b) Y. Deng, X. Feng, D. Yang, C. Yi, X. Qiu, *BioResources* **2012**, *7*, 1145–1156.
- [27] a) J. L. Li, B. Yuan, X. Y. Liu, H. Y. Xu, *Cryst. Growth Des.* **2010**, *10*, 2699–2706; b) M. A. Rogers, A. G. Marangoni, *Cryst. Growth Des.* **2008**, *8*, 4596–4601.
- [28] Z. Wei, Z. Y. Gu, R. K. Arvapally, Y. P. Chen, R. N. McDougald, J. F. Ivy, A. A. Yakovenko, D. Feng, M. A. Omary, H. C. Zhou, *J. Am. Chem. Soc.* **2014**, *136*, 8269–8276.

- [29] J. Yang, Z. C. Ren, B. Chen, M. M. Fang, Z. J. Zhao, B. Z. Tang, Q. Peng, Z. Li, *J. Mater. Chem. C* **2017**, *5*, 9242–9246.
- [30] A. Maliakal, G. Lem, N. J. Turro, R. Ravichandran, J. C. Suhadolnik, A. D. DeBellis, M. G. Wood, J. Lau, *J. Phys. Chem. A* **2002**, *106*, 7680–7689.
- [31] J. R. Lakowicz, *Principles of Fluorescence Spectroscopy*, 3rd ed., Springer, New York, **2006**.
- [32] J. Keizer, *J. Am. Chem. Soc.* **1983**, *105*, 1494–1498.
- [33] a) Q. Zhang, J. Su, D. Feng, Z. Wei, X. Zou, H. Zhou, *J. Am. Chem. Soc.* **2015**, *137*, 10064–10067; b) W. Miao, L. Qin, D. Yang, X. Jin, M. Liu, *Chem. Eur. J.* **2015**, *21*, 1064–1072.
- [34] P. I. Djurovich, E. I. Mayo, S. R. Forrest, M. E. Thompson, *Org. Electron.* **2009**, *10*, 515–520.
- [35] J. Y. Chen, B. Yuan, Z. Y. Li, B. Tang, E. Ankers, X. G. Wang, J. L. Li, *Langmuir* **2016**, *32*, 1171–1177.

Manuscript received: June 20, 2018

Revised manuscript received: August 2, 2018

Accepted manuscript online: August 3, 2018

Version of record online: September 16, 2018